Journal of Alloys and Compounds 569 (2013) 76–81

Contents lists available at SciVerse ScienceDirect

Journal of Alloys and Compounds

journal homepage: www.elsevier.com/locate/jalcom

Study on structure and electrochemical properties of carbon-coated monoclinic $Li_3V_2(PO_4)_3$ using synchrotron based *in situ* X-ray diffraction and absorption

Jeongbae Yoon [a], Shoaib Muhammad [a], Donghyuk Jang [a], N. Sivakumar [b], Jaeyoon Kim [a], Won-Hee Jang [c], Yun-Sung Lee [c,*], Young-Uk Park [d], Kisuk Kang [d], Won-Sub Yoon [a,*]

[a] Department of Energy Science, Sungkyunkwan University, 300 Suwon-si, Gyeonggi-do 440-746, Republic of Korea
[b] School of Advanced Materials Engineering, Kookmin University, 861-1 Jeongneung-dong, Seongbuk-gu, Seoul 136-702, Republic of Korea
[c] Faculty of Applied Chemical Engineering, Chonnam National University, Gwang-ju 500-757, Republic of Korea
[d] Department of Materials Science and Engineering, Seoul National University (SNU), Seoul 151-744, Republic of Korea

ARTICLE INFO

Article history:
Received 19 February 2013
Received in revised form 20 March 2013
Accepted 21 March 2013
Available online 27 March 2013

Keywords:
Lithium battery
Cathode materials
Lithium vanadium phosphate
In situ XRD
In situ XAS

ABSTRACT

Monoclinic $Li_3V_2(PO_4)_3$ is a highly promising cathode material for lithium–ion rechargeable batteries. It has good ion mobility and high lithium capacity due to its ability to reversibly extract all three lithium ions. Here, we present, a systematic investigation of phase transitions and volume variations that occur during lithium extraction from the carbon-coated monoclinic phase of $Li_3V_2(PO_4)_3$ by synchrotron based *in situ* X-ray diffraction and X-ray absorption spectroscopy. This monoclinic $Li_3V_2(PO_4)_3$ illustrates complex behavior of four successive two-phase transitions upon extraction of all three lithium ions between 3.0 and 4.8 V vs. Li/Li^+. Each XRD pattern of the intermediate compositions can be fully indexed in the monoclinic space group $P2_1/n$, with net volume reduction of 6.47%. *In situ V K-edge* XANES in combination with study of structural parameters is applied to find the vanadium valence state at plateau regions, which highlights the variations in electrochemical potential constraining to extraction of lithium ion from different crystal sites.

1. Introduction

Rechargeable lithium–ion batteries are sophisticated electrical energy storage and transfer system for modern electronic applications such as cellular phones, notebook computers, and electric vehicles, due to their high energy density and long cycle life. Commercial cells make use of cobalt based oxides as the positive electrode, but high cost and toxicity prohibited its use in large-scale applications [1]. Safety, energy density, cost and rate performance are major challenges faced by lithium ion batteries [2,3]. In recent decades, alternative material family of lithium transition metal phosphates including $LiCoPO_4$, $LiFePO_4$, $LiMnPO_4$, $Li_3V_2(PO_4)_3$ and multicomponent olivines has fascinated the researchers due to high operational potential and thermal stabilities [4–12]. Among the phosphates mentioned above, lithium vanadium phosphate has attracted significant attention as cathode material because of high reversible capacity. $Li_3V_2(PO_4)_3$ can be crystallized in two different structures: (i) the rhombohedral (NASICON) phase and (ii) thermodynamically more stable monoclinic phase. The monoclinic $Li_3V_2(PO_4)_3$ is a highly promising material, proposed as cathode for higher voltage rechargeable lithium–ion batteries due to its stable framework and good ion mobility [13,14]. Monoclinic $Li_3V_2(PO_4)_3$ (space group $P2_1/n$) contains three fourfold crystallographic positions for lithium in the framework of metal octahedron and phosphate tetrahedron sharing oxygen vertices. Each VO_6 octahedron is surrounded by six PO_4 tetrahedrons, whereas each PO_4 tetrahedron is surrounded by four VO_6 octahedrons, and this leads to the formation of three-dimensional network that permits rapid lithium ion diffusion [14]. The theoretical capacity of $Li_3V_2(PO_4)_3$ is 197 mA h/g, when all the three Li ions are completely extracted at 4.8 V, which is the highest for all phosphates [15,16]. Two lithium ions can be extracted and reinserted reversibly between 3.0 and 4.3 V based on the V^{3+}/V^{4+} redox couple. In the monoclinic $Li_3V_2(PO_4)_3$ phase, the first charging voltage (3.61–3.68 V) is associated with the presence of an ordered Li phase of intermediate composition $Li_{2.5}V_2(PO_4)_3$ and then the second stage (3.68–4.1 V) is related to the removal of Li–ions from the stable tetrahedral sites. Then, the final stage (4.1–4.5 V) is due to the change of the V^{3+}/V^{4+} redox couple to the $V^{4+/5+}$ redox couple [14]. Upon charging to 4.8 V, all three lithium ions can be fully extracted and reversibly intercalated at high rate. Morcrette et al. [17], studied the lithium

* Corresponding authors. Tel.: +82 31 299 6276; fax: +82 82 31 299 4279 (W.-S. Yoon).
E-mail addresses: leeys@chonnam.ac.kr (Y.-S. Lee), wsyoon@skku.edu (W.-S. Yoon).

0925-8388/$ - see front matter © 2013 Elsevier B.V. All rights reserved.
http://dx.doi.org/10.1016/j.jallcom.2013.03.188

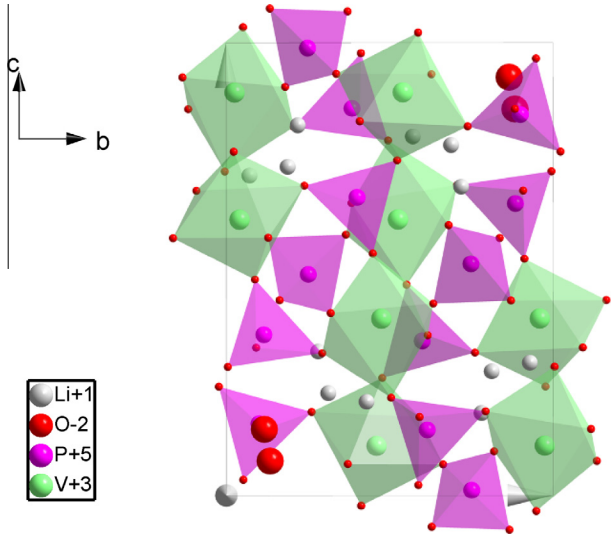

Fig. 1. Schematic illustration of the crystal structure of $Li_3V_2(PO_4)_3$.

Table 1
Atomic sites (number of positions and Wyckoff notation) and coordinates *x*, *y*, *z* (in units of lattice constants (a = 8.6098 Å, b = 8.5950 Å, c = 12.0431 Å, β = 90.5899°) of $Li_3V_2(PO_4)_3$ coated with adipic acid. The weighted factor R_{wp} = 12.04%.

Atom	*x*	*y*	*z*	Occupancy
Li_1 (4e)	0.2087(0)	0.7775(7)	0.1796(4)	1.0
Li_2 (4e)	0.9234(6)	0.3032(9)	0.2415(3)	1.0
Li_3 (4e)	0.5722(7)	0.4121(0)	0.1923(0)	1.0
V_1 (4e)	0.2475(7)	0.4610(0)	0.1101(5)	1.0
V_2 (4e)	0.7519(7)	0.4716(4)	0.3899(2)	1.0
P_1 (4e)	0.1064(7)	0.1027(4)	0.1486(0)	1.0
P_2 (4e)	0.6038(9)	0.1152(3)	0.3527(0)	1.0
P_3 (4e)	0.0361(2)	0.2489(1)	0.4919(0)	1.0
O_1 (4e)	0.9273(9)	0.1120(2)	0.1468(2)	1.0
O_2 (4e)	0.1446(8)	0.9809(3)	0.2385(8)	1.0
O_3 (4e)	0.1751(9)	0.0509(9)	0.0422(2)	1.0
O_4 (4e)	0.1615(6)	0.2644(1)	0.1867(8)	1.0
O_5 (4e)	0.4311(0)	0.0889(0)	0.3301(0)	1.0
O_6 (4e)	0.6982(4)	−0.0021(9)	0.2805(4)	1.0
O_7 (4e)	0.6436(4)	0.0882(4)	0.4734(1)	1.0
O_8 (4e)	0.6422(3)	0.2854(7)	0.3181(1)	1.0
O_9 (4e)	0.9509(9)	0.1336(0)	0.5673(8)	1.0
O_{10} (4e)	0.9286(5)	0.3187(5)	0.4042(4)	1.0
O_{11} (4e)	0.1690(7)	0.1687(7)	0.4296(8)	1.0
O_{12} (4e)	0.1095(8)	0.3668(1)	0.5727(1)	1.0

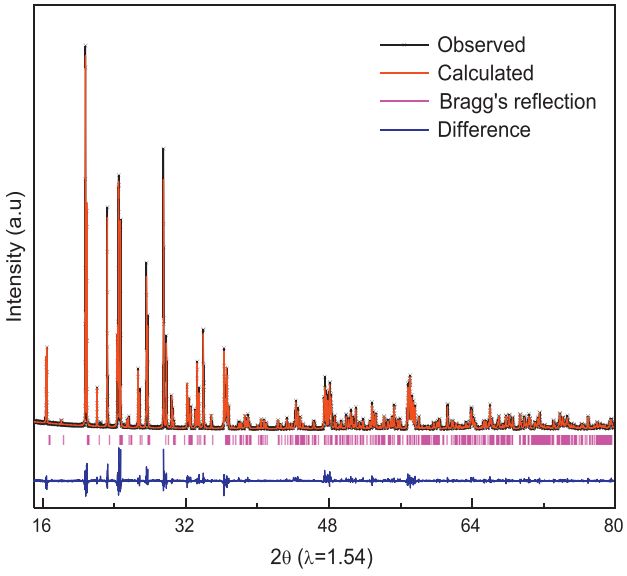

Fig. 2. Observed, calculated and difference plots obtained for $Li_3V_2(PO_4)_3$ cathode sample from Rietveld refinement of the powder XRD patterns.

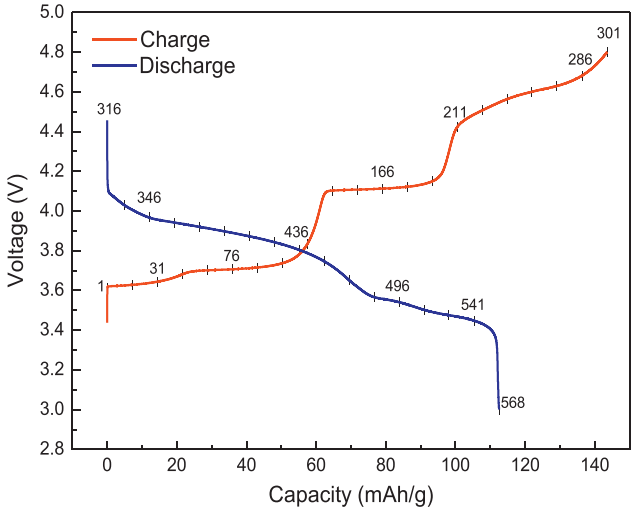

Fig. 3. The first charge/discharge curve of carbon-coated $Li_3V_2(PO_4)_3$ during charging at C/20 rate at 4.8 V.

extraction from rhombohedral and monoclinic $Li_3V_2(PO_4)_3$ using *in situ* X-ray diffraction and reported extraction of all the three lithium ions from $Li_3V_2(PO_4)_2$. Lee and Park [18] have used computational methods to characterize the structure and concluded that lithium ion mobility in monoclinic $Li_3V_2(PO_4)_3$ is high enough to exhibit good performance as cathode material. Cho et al. [19] have shown significantly high discharge capacity of 182 mA h/g by Al doping and carbon coating. Moreover, monoclinic $Li_3V_2(PO_4)_3$ can also demonstrate high rate capability by adopting novel synthesis techniques and surface coating [20–22].

Rate capability and high discharge capacity are major electrochemical characteristics of lithium ion secondary battery required for power storage applications. Limited intercalation/deintercalation dynamics are usually due to poor conductivity of electrode material. Doping of alien cations, designing of nanoparticle and composite electrode are feasible ways to enhance the intrinsic conductivity and boost the overall performance of electrode materials [23–28]. Similarly, addition of carbon can also effectively increase the electrode conductivity, improve the surface chemistry and protect the electrode from direct contact with electrolyte to enhance the cycle life. Fine layer of carbon on grain boundary can be achieved by pyrolysis of organic precursors such as aniline or adipic acid during the sample synthesis [29,30]. However, to the best of our knowledge, there were no reports available about the structural changes of carbon-coated monoclinic lithium vanadium phosphate during electrochemical cycling. One of the key problems related to the electrochemical performance of electrode materials for lithium ion battery was phase transitions and local structure changes during lithium insertion or extraction. *In situ* XRD study of lithium ion battery is a comprehensive tool to track phase transitions of electrode material and XAS has been successfully employed to study local structure changes [31,32]. In the present work, electrochemical properties of carbon-coated monoclinic $Li_3V_2(PO_4)_3$ as a cathode material, its structural changes and

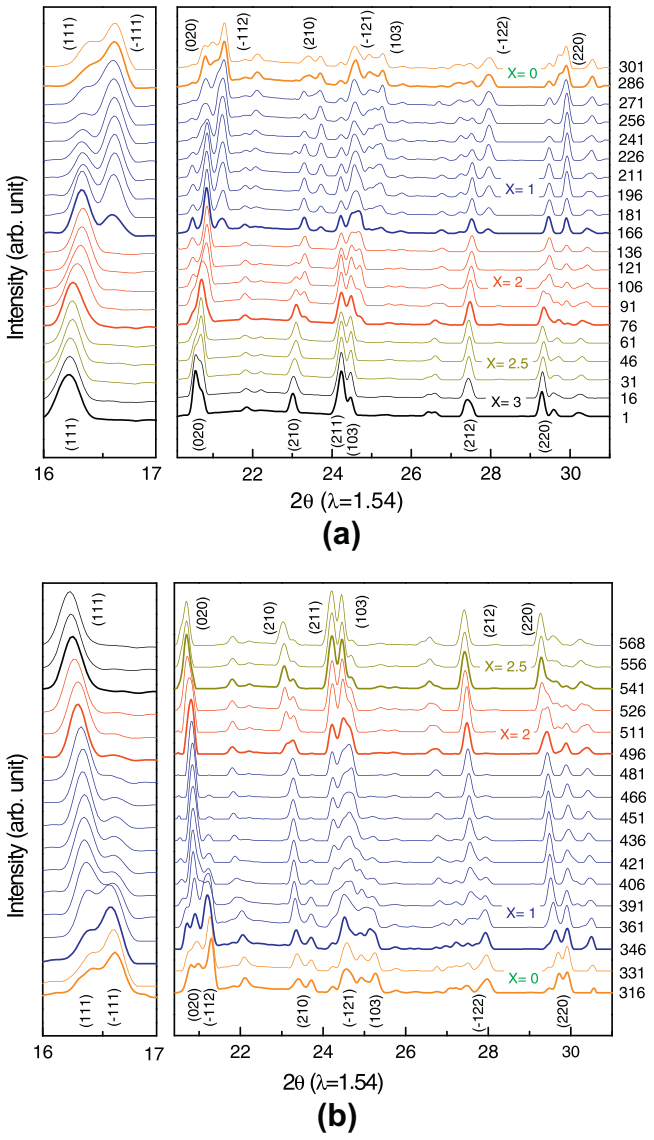

Fig. 4. The *in situ* XRD patterns of prepared (a) $Li_3V_2(PO_4)_3$ sample during the first charge; (b) discharging at C/20 rate.

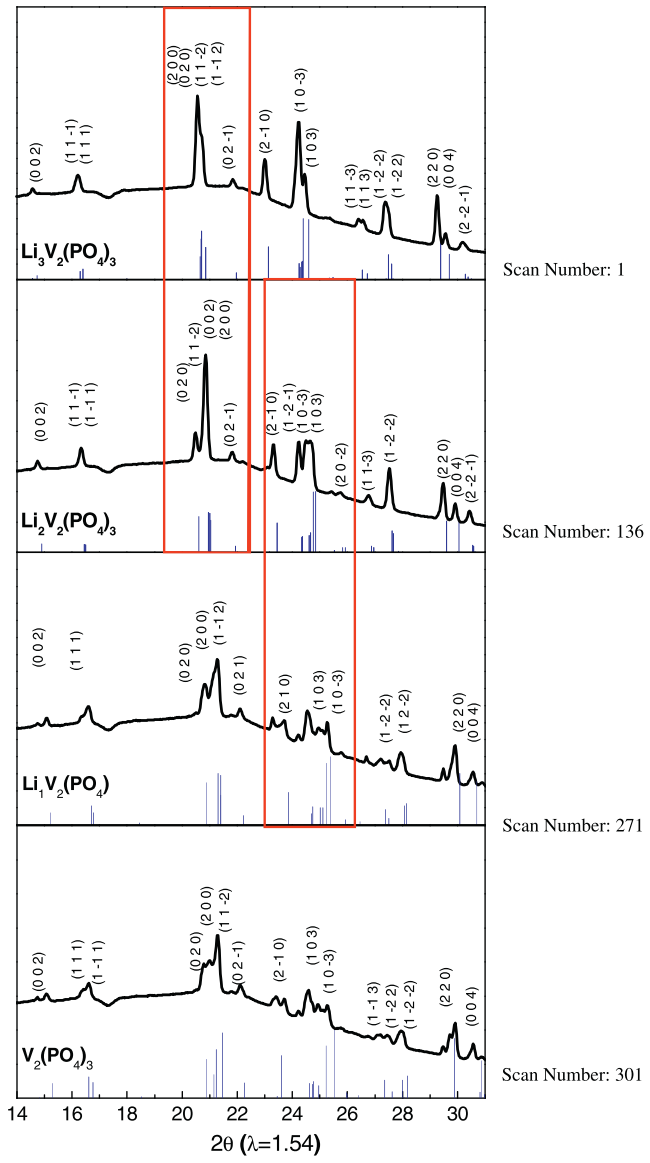

Fig. 5. Selected XRD patterns of $Li_3V_2(PO_4)_3$ cathode samples at different values of x in $Li_{3-x}V_2(PO_4)_3$ where (x = 0, 1, 2 and 3).

Table 2
Lattice parameters of each phase of $Li_xV_2(PO_4)_3$ cathode where (x = 3, 2.5, 2, 1) during first charge, calculated from least-square fitting.

Phase	a (Å)	b (Å)	c (Å)	β (°)	Cell volume (Å^3)
$Li_3V_2(PO_4)_3$	8.603	8.588	12.035	90.58	889.17
$Li_{2.5}V_2(PO_4)_3$	8.549	8.607	11.983	90.05	881.79
$Li_2V_2(PO_4)_3$	8.468	8.612	11.901	90.28	867.89
$Li_1V_2(PO_4)_3$	8.301	8.528	11.652	89.64	824.84
$V_2(PO_4)_3$	8.388	8.507	11.650	89.09	831.63

stability of crystal structure have been investigated during charging/discharging using synchrotron based *in situ* X-ray diffraction (XRD) and X-ray absorption (XAS) techniques.

2. Experimental

The monoclinic $Li_3V_2(PO_4)_3$ was prepared by using conventional solid-state route. High purity $LiCO_3$ (Wako, Japan), V_2O_5 (Sigma–Aldrich, USA), $(NH_4)_2HPO_4$ (Sigma–Aldrich, USA) and $C_6H_{10}O_4$ (Sigma–Aldrich, USA) were used. These starting materials were mixed in stoichiometric amounts, with adipic acid (molar ratio of adipic acid to total metal ions was 0.15) to synthesize the carbon-coated $Li_3V_2(PO_4)_3$. The resultant mixture was ground thoroughly and sintered at 900 °C for 8 h under argon atmosphere using tubular furnace to obtain the $Li_3V_2(PO_4)_3$ cathode samples.

Cathodes were prepared by slurring the active material powder with 10 wt.% Super-P and 10 wt.% poly-vinylidene fluoride (PVDF) in N-methyl pyrrolidone (NMP) solvent, then coating the mixture onto Al foil. The cathodes were packed in the cells with a lithium metal foil as a negative electrode and a Celgard separator. The electrolyte used was $LiPF_6$ (1.3 M) in *a* 3:7 ethyl carbonate/dimethyl carbonate (EC/DMC) solution. The cell was assembled in an argon-filled glove box. The detailed design of the spectroelectrochemical cell used in the *in situ* XRD and XAS measurements has been described elsewhere [33]. Powder XRD patterns were collected at beamline 9B(HRPD) Pohang Accelerator Laboratory. *In situ* XRD patterns were collected at beamline 1D (KIST-PAL) Pohang Accelerator Laboratory using MAR 345-image plate detector. The wavelengths used were 0.9999 Å. The two theta angles for all the XRD patterns existing in this paper have been recalculated and changed to the corresponding angles for λ = 1.54 Å, which is the wavelength of a conventional X-ray tube source with Cu Kα radiation, for easy comparison with data in other publications. *In situ* XAS spectra were collected in transmission mode at beamline 10C in Pohang Accelerator Laboratory.

3. Results and discussion

The schematic illustration of monoclinic $P2_1/n$ structure of $Li_3V_2(PO_4)_3$ is shown in Fig. 1. The three-dimensional network

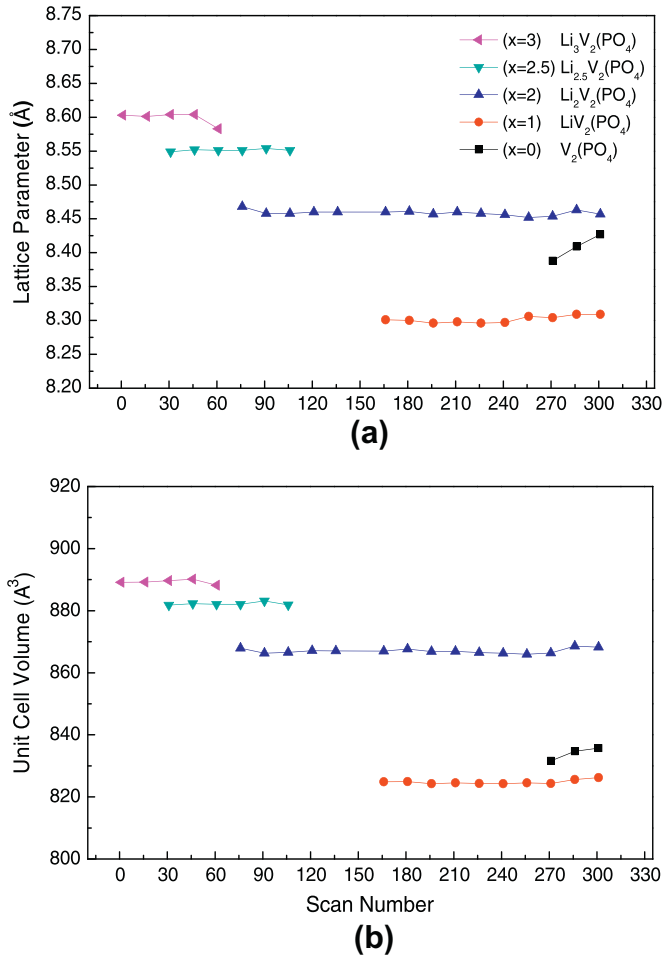

Fig. 6. Variation of lattice parameter and volume in $Li_xV_2(PO_4)_3$ ($0 < x < 3$) during first charge.

consisted of slightly distorted vanadium octahedra and phosphorus tetrahedra linked together via common apical oxygen atoms to form a $(V–O–P–O)_n$ bonding arrangement. Three distinct lithium atoms occupied three distinct crystallographic positions in the interstitial voids. Li(1) is surrounded by four oxygen atoms to form a tetrahedron, Li(2) and Li(3) occupied highly distorted tetrahedral environments that can be better described as 5-coordinate Li–O sites, where the fifth Li–O bond is long (ca. 2.6 Å). The occurrence of corner-shared chains of Li polyhedral along the *b*-axis and open diffusion pathways in the other directions directed rapid, isotropic ionic transport similar to the fast-ion conduction in NASICON phases.

The initial characterization of the material was carried out using powder X-ray diffraction (XRD). Since small amount of impurities affect the electrochemical properties, more precise XRD patterns are preferred for better characterization of material. Rietveld refinement of these XRD patterns was carried out using powder XRD data in order to confirm the formation of monoclinic $Li_3V_2(PO_4)_3$. Fig. 2 showed the XRD pattern together with the Rietveld refinement based on single crystal data for $Li_3V_2(PO_4)_3$ compound. The diffraction peaks of $Li_3V_2(PO_4)_3$ powder corresponded to a single-phase, indexed with monoclinic structure and no impurity phase was detected. A space group of $P2_1/n$ is preferred as the refinement model. Refined unit-cell parameters are $a = 8.6098$ Å, $b = 8.5950$ Å, $c = 12.0431$ Å, $\beta = 90.5899°$ and $V = 891.159$ Å^3 which were consistent with those in previous reports [14,15]. In this monoclinic structure, each unit cell contains four chemical formula units of $Li_3V_2(PO_4)_3$, all the Li, V, P, and O atoms occupied Wyckoff position 4e with different coordinates. The atomic parameters of $Li_3V_2(PO_4)_3$ are given in Table 1. The monoclinic structure comprised of metal octahedra and phosphate tetrahedra sharing oxygen vertices. The electric charge carriers, lithium ions, are situated in the cavities within the framework. The three crystallographic independent Li sites in $Li_3V_2(PO_4)_3$: Li_1, Li_2, and Li_3 were 4-, 5- and 5-coordinate, respectively. Three fourfold crystallographic positions present for the Li atoms led to 12 lithium positions within the unit cell. Huang et al. [34], have reported that three

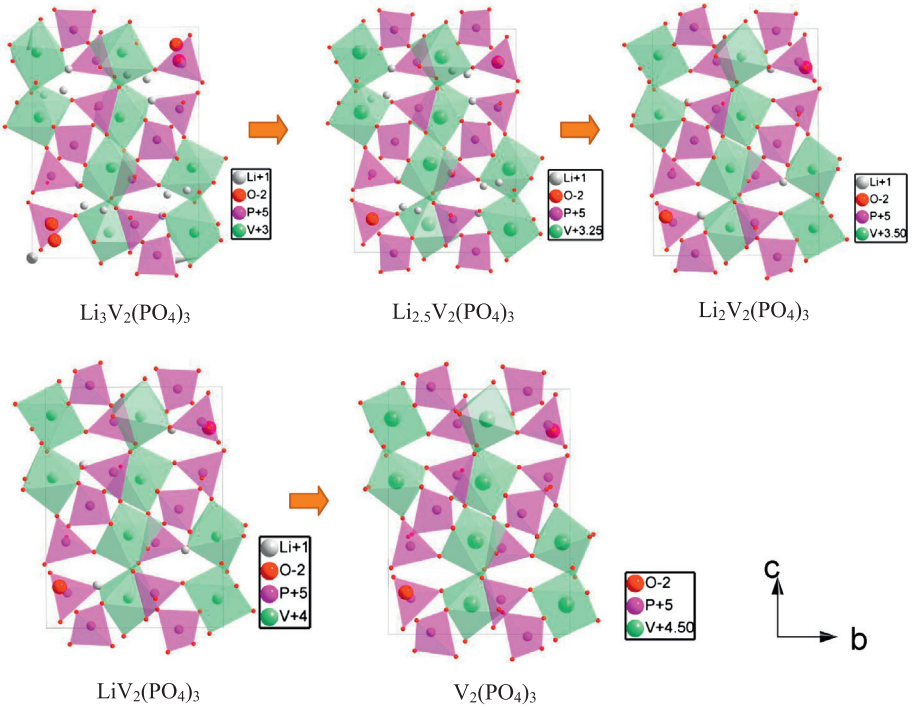

Fig. 7. Schematic illustration of the crystal structure of $Li_3V_2(PO_4)_3$, projected along *b*-axis during first charging.

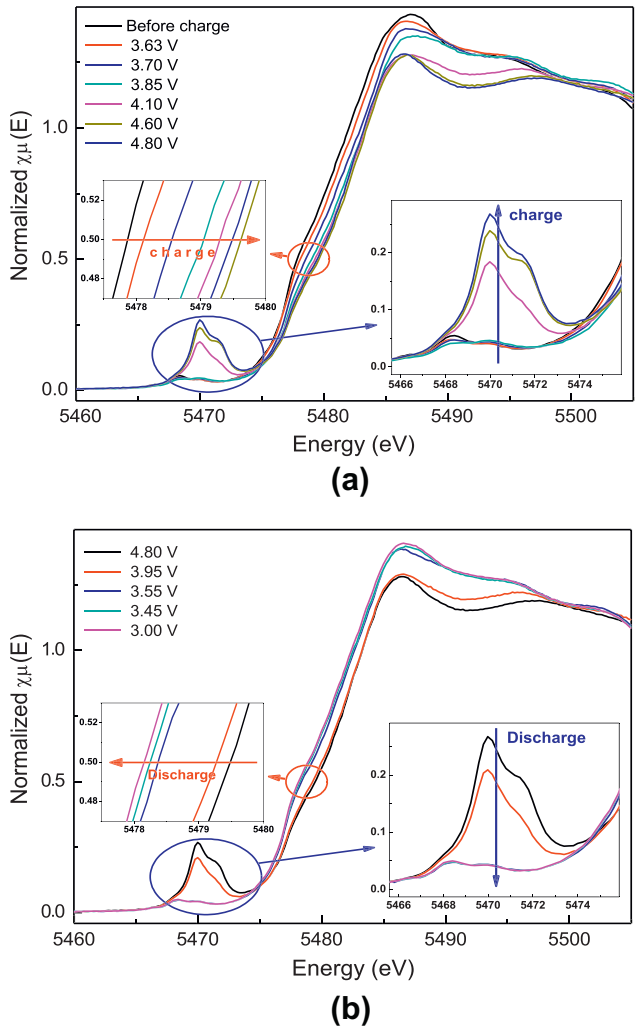

Fig. 8. Normalized *in situ V K-edge* XANES spectra of $Li_3V_2(PO_4)_3$ cathode, during the first (a) charge and (b) discharge.

dimensional structure allows reversible extraction of all three lithium ions from the monoclinic vanadium phosphate at different rates depending on the site of Li ion.

Fig. 3 shows the first cycle charge/discharge curves of carbon-coated $Li_3V_2(PO_4)_3$ cathode material between 3.0 to 4.8 V at C/20 rate. In the first cycle, the charge capacity achieved at 4.8 V was 143 mA hg^{-1} and discharge capacity reached at 3.0 V was 112 mA hg^{-1}. Charge/discharge capacity was lower than the previously published results mainly due to design limitations of the *in situ* cell. Three plateau regions during the charging process can be ascribed as $V^{3+}/V^{4+}/V^{5+}$. The selected XRD scan numbers are marked on the charge and discharge curves. The vertical bars on the curves indicated the start of each scan. 301 scans of XRD spectra were collected during charging to 4.8 V and 252 more scans were collected during subsequent discharging period.

Fig. 4 shows the selected *in situ* XRD patterns of $Li_3V_2(PO_4)_3$ cathode sample which were collected during cycling at C/20 rate. The numbers marked beside the patterns correspond to the scan numbers in Fig. 3. Each XRD pattern was completely indexed in the monoclinic space group $P2_1/n$ (unique axis b) with $a = 8.60(9)$; $b = 8.59(5)$; $c = 12.04(3)$ and $\beta = 90.5(8)^\circ$ for the starting $Li_3V_2(PO_4)_3$ phase. The structure marked as "$x = 3$" was for $Li_3V_2(PO_4)_3$ before charge that shows the same NASICON structured phase with trigonal bipyramidal environment as reported by Morgan et al. [35]. Upon charging (i.e. lithium extraction), replacing the pristine phase 1, new NASICON-like phase are observed during lithium extraction, illuminating two-phase reaction mechanism in certain lithium composition ranges as shown in Fig. 4a. The Bragg peaks from both the phases were very close to each other, indicating very similar lattice parameters.

The *in situ* XRD patterns recorded upon oxidation from $Li_3V_2(PO_4)_3$ to $V_2(PO_4)_3$ established the sequence of two-phase processes during the electrochemical charging cycle. Volume reduction of the structure was prominent ($\Delta V = -1.57\%$) for the second plateau at 3.67 V between $Li_{2.5}V_2(PO_4)_3$ and $Li_2V_2(PO_4)_3$ as listed in Table 2. Upon further Li extraction, between $Li_2V_2(PO_4)_3$ and $LiV_2(PO_4)_3$, a third two-phase process was encountered at 4.06 V vs. Li/Li^+ with a more noticeable unit cell volume reduction ($\Delta V = -4.96\%$). Therefore, the two-phase process was evidently confirmed at intermediate x values ($0 < x < 2$) in $Li_xV_2(PO_4)_3$, for which the diffraction patterns exhibit the peaks of both $Li_3V_2(PO_4)_3$ and $LiV_2(PO_4)_3$. These diffraction patterns were identified and indexed based on full pattern matching as shown in Fig. 5. As a result of oxidation of V^{3+}/V^{4+} and extraction of two lithium ions between $Li_3V_2(PO_4)_3$ and $Li_1V_2(PO_4)_3$, the overall unit cell volume reduction ($\Delta V = -7.23\%$) was in good agreement with the results ($\Delta V = -6.8\%$) of Morcrette et al. [17]. Unit cell volume reduction was fairly significant but it does not produce irreversibility of the electrochemical reactions. Many reporters observed stable capacity on cycling between 3.0 and 4.2 V vs. Li/Li^+ [36,37]. The fourth step, at higher voltage (~4.45 V vs. Li/Li^+), corresponded to the oxidation part of $V^{4+}/^{5+}$, again as a two-phase reaction between $LiV_2(PO_4)_3$ and $V_2(PO_4)_3$. In this reaction, we observed a much stronger polarization of the cell on charge as the apparent voltage rise at around 4.6 V, even with a slow current rate. The end member $V_2(PO_4)_3$ is characterized clearly, by a bigger unit-cell volume (831.6 $Å^3$) than $LiV_2(PO_4)_3$ (824.6 $Å^3$) as shown in Table 2.

The new phase evolution occurs by Li reordering during charging, as shown in schematic diagram in Fig. 7. From the experimental electrochemical data and *in situ* XRD patterns, it is clear that complicated mixing between solid solution process exists and two-phase reaction is involved on discharge between $V_2(PO_4)_3$ and $Li_2V_2(PO_4)_3$. Moreover, it was evident from Fig. 4b that the fully discharged phase is not same as the pristine phase of $Li_3V_2(PO_4)_3$, instead it exhibited a mixed phase. After first cycle fully discharged cathode returns to $Li_{2.5}V_2(PO_4)_3$ phase at 3.0 V. The variation of lattice parameters and volume of $Li_xV_2(PO_4)_3$ ($0 < x < 3$) during first charging is shown in Fig. 6. Refinement of lattice parameters by full pattern matching indicated that $Li_{2.5}V_2(PO_4)_3$ possesses slightly smaller unit cell ($\Delta V = -0.89\%$) as compared to pristine, comparison can be found in Table 2. Variations in unit cell volume were not uniform with state of charge. Li(3) and Li(2) are displaced from 5-coordination region, whereas third lithium ion, removed at 4.8 V, lies in stable tetrahedral environment. This complex geometry was responsible for nonlinear volume changes and difference in potentials required to remove three lithium ions from $Li_3V_2(PO_4)_3$.

In order to confirm the oxidation state of vanadium in $Li_3V_2(PO_4)_3$ during charging, metallic *V K-edge* XANES data was recorded as shown in Fig. 8. In general, the shape of *K*-edge XANES data of transition metal oxides provides unique information about site symmetry and the nature of bonding with surrounding ligands, while the threshold energy position of the absorption edge gives information about the oxidation state of the probing atom [38–40]. Higher absorption energy is required to excite 1s core electron of the higher oxidation ion, which is more strongly bounded to less screened nucleus. So, major edge shift to higher energy in the *V K-edge* XANES spectra indicated increase in the average oxidation state of this element [41]. Fig. 8a shows the edge shift in *V K-edge* region toward higher energy positions during charging indicated

the increase of oxidation states of the V ions in $Li_3V_2(PO_4)_2$ cathode upon delithiation. During discharging, energy position of *V K-edge* XANES spectra shifted back towards lower energy regions which is shown in the Fig. 8b [42]. The XANES results showed that the average valence of V in fully discharged $Li_3V_2(PO_4)_2$ cathode material is higher than that of pristine cathode, which is in good accordance with *in situ* XRD results.

4. Conclusions

In this work, we studied the structural properties of carbon-coated monoclinic $Li_3V_2(PO_4)_3$ using synchrotron based *in situ* X-ray diffraction. In spite of complex phase transformations, we followed the four successive two-phase transitions during extraction/insertion of lithium ion from monoclinic $Li_3V_2(PO_4)_3$ to $V_2(PO_4)_3$. From the electrochemical and *in situ* XRD results, it is concluded that monoclinic $Li_3V_2(PO_4)_3$ maintains its structural integrity during the cycling despite two phase reaction mechanism and large volume changes in the unit cell. Nonlinear volume changes during battery charging suggested that removal of first lithium ion from perfect tetrahedral sites requires more energy. *In situ V K-edge* XANES results exposed that fully discharged $Li_3V_2(PO_4)_3$ cathode material exhibits mixed two phases unlike the pristine cathode material with pure single phase.

Acknowledgments

This work was supported by the Fundamental R&D Program for Technology of World Premier Materials and Energy Efficiency & Resources (2010T100200295) of Ministry of Knowledge Economy. This work was partly supported by the National Research Foundation funded by the Korean Government (MEST: NRF- 2010-0029065 & R31-2008-10029).

References

[1] M. Dubarry, C. Truchot, M. Cugnet, C. Michelbacher, J. Power Sources 196 (2011) 10328.
[2] J.B. Goodenough, J. Solid State Electrochem. 16 (2012) 2019.
[3] N.-S. Choi, Z. Chen, S.A. Freunberger, P.G. Bruce, Angew. Chem. Int. Ed. 51 (2012) 9994.
[4] V. Aravindan, J. Gnanaraj, Y.-S. Lee, S. Madhavi, J. Mater. Chem. A 1 (2013) 3518.
[5] Z. Gong, Y. Yang, Energy Environ. Sci. 4 (2011) 3223.
[6] A.V. Murugan, T. Muraliganth, A. Manthiram, J. Electrochem. Soc. 156 (2009) A79.
[7] M. Konarova, I. Taniguchi, J. Power Sources 195 (2010) 3661.
[8] S.-M. Oh, S.-W. Oh, C.-S. Yoon, B. Scrosati, K. Amine, Y.-K. Sun, Adv. Funct. Mater. 20 (2010) 3260.
[9] Q. Zhang, S. Zhong, L. Liu, J. Liu, J. Jiang, J. Wang, Y. Li, J. Phys. Chem. Solids 70 (2009) 1080.
[10] R.K.B. Gover, A. Bryan, P. Burns, J. Barker, Solid State Ionics 177 (2006) 1495.
[11] Y.-U. Park, R.A. Shakoor, K.-Y. Park, K. Kang, J. Electrochem. Sci. Technol. 2 (2011) 14.
[12] C.G. Son, D.R. Chang, H.S. Kim, Y.S. Lee, J. Electrochem. Sci. Technol. 2 (2011) 103.
[13] S.-C. Yin, H. Grondey, P. Strobel, H. Huang, L.F. Nazar, J. Am. Chem. Soc. 125 (2003) 326.
[14] S.-C. Yin, H. Grondey, P. Strobel, M. Anne, L.F. Nazar, J. Am. Chem. Soc. 125 (2003) 10402.
[15] X.J. Zhu, Y.X. Liu, L.M. Geng, L.B. Chen, J. Power Sources 184 (2008) 578.
[16] H.-H. Lim, A.-R. Cho, N. Sivakumar, W.-S. Kim, W.-S. Yoon, Y.-S. Lee, Bull. Korean. Chem. Soc. 32 (5) (2011) 1.
[17] M. Morcrette, J.-B. Leriche, S. Patoux, C. Wurm, C. Masquelier, Electrochem. Solid-State Lett. 6 (2003) A80.
[18] S. Lee, S.S. Park, J. Phys. Chem. C 116 (2012) 25190.
[19] A.R. Cho, J.N. Son, V. Aravindan, W.S. Yoon, Y.S. Lee, J. Mater. Chem. 22 (2012) 6556.
[20] F. Wu, F. Wang, C. Wu, Y. Bai, J. Alloys Comp. 513 (2012) 236.
[21] Q. Chen, T. Zhang, X. Qiao, D. Li, J. Yang, J. Power Sources 234 (2013) 197.
[22] J. Zhai, M. Zhao, D. Wang, Y. Qiao, J. Alloys Comp. 502 (2010) 401.
[23] Y. Zhang, Q.-Y. Huo, Y. Lv, L.-Z. Wang, H.-C. Dong, J. Alloys Comp. 542 (2012) 187.
[24] J. Yao, S. Wei, P. Zhang, C. Shen, K.-F. Aguey-Zinsou, L. Wang, J. Alloys Comp. 532 (2012) 49.
[25] T. Jiang, Y.J. Wei, W.C. Pan, C.Z. Wang, J. Alloys Comp. 488 (2009) L26.
[26] Y.Q. Qiao, J.P. Tu, Y.J. Mai, C.D. Gu, J. Alloys Comp. 509 (2011) 7181.
[27] Y.Q. Qiao, X.L. Wang, C.D. Gu, J.P. Tu, J. Alloys Comp. 536 (2012) 132.
[28] H. Liu, S. Bi, G. Wen, F. Zhang, J. Alloys Comp. 543 (2012) 99.
[29] H. Li, H. Zhou, Chem. Commun. 48 (2012) 1201.
[30] L.-L. Zhang, Y. Li, G. Peng, J. Ma, Y.-H. Huang, J. Alloys Comp. 513 (2012) 414.
[31] S. Lee, D. Jang, J. Yoon, Y.-H. Cho, Y.-S. Lee, D.-H. Kim, W.-S. Kim, W.-S. Yoon, J. Electrochem. Sci. Technol. 3 (2012) 29.
[32] W.-S. Yoon, C.P. Grey, M. Balasubarmanium, X.-Q. Yang, J. McBreen, Chem. Mater. 15 (2003) 3161.
[33] M. Balasubramanian, X. Sun, X.Q. Yang, J. McBreen, J. Power Sources 92 (2001) 1.
[34] H. Huang, S.C. Yin, T. Kerr, N. Talor, L.F. Nazar, Adv. Mater. 14 (2002) 1525.
[35] D. Morgan, G. Ceder, M.Y. Saidi, J. Swoyer, H. Huang, G. Adamson, Chem. Mater. 14 (2002) 4684.
[36] S. Patoux, C. Wurm, M. Morcrette, G. Rousse, C. Masquelier, J. Power Sources 119 (2003) 278.
[37] M.Y. Saidi, J. Barker, H. Huang, J.L. Swoyer, G. Adamson, J. Power Sources 119 (2003) 266.
[38] K.-W. Nam, W.-S. Yoon, K. Zaghib, K.Y. Chung, X.-Q. Yang, Electrochem. Commun. 11 (2009) 2023.
[39] J.-M. Kim, H.-T. Chung, Electrochim. Acta 49 (2004) 937.
[40] K.-W. Nam, X.-J. Wang, W.-S. Yoon, H. Li, X. Huang, O. Hass, J. Bai, X.-Q. Yang, Electrochem. Commun. 11 (2009) 913.
[41] M. Pivko, I. Arcon, M. Bele, R. Dominko, M. Gaberscek, J. Power Sources 216 (2012) 145.
[42] L.-L. Zhang, G. Liang, A. Iganatov, M. Croft, Y.-L. Peng, J. Phys. Chem. C. 115 (2011) 13527.